PHYSICAL REVIEW C VOLUME 2, NUMBER 5 NOVEMBER 1970

Resonance Neutron Capture in Rh^{103}†

K. Rimawi* and J. B. Garg
Department of Physics, State University of New York, Albany, New York 12203

and

R. E. Chrien and R. G. Graves
Brookhaven National Laboratory, Upton, New York 11973
(Received 14 April 1970)

The γ-ray spectra following slow-neutron capture in a target of Rh^{103} have been measured with the fast-chopper time-of-flight facility at the high flux beam reactor at Brookhaven National Laboratory. A total of 145 radiative intensities, involving transitions from seven resonances and 16 unresolved resonances, to levels in Rh^{104} have been recorded. A neutron binding energy of 6999.3 ± 1.5 keV is obtained. From these high-energy γ-ray data, several spin assignments for levels in Rh^{104} are made. The distribution of transition probabilities in rhodium is not consistent with the Porter-Thomas distribution; values of $\nu = 2.70^{+0.53}_{-0.40}$ and $\nu = 2.45^{+0.38}_{-0.40}$ are obtained as best fits to the class of χ^2 distribution functions to spin-0 and spin-1 resonances, respectively. The gross shape of the γ-ray spectrum shows an enhancement of strength to states near 1 MeV in excitation energy, both for thermal and resonance capture. It is shown that this enhancement is not due to a direct-reaction process, and it is suggested that the presence of doorway states may be responsible for this enhancement.

I. INTRODUCTION

The level density of the odd-odd nucleus Rh^{104} is expected to be very high at low excitation energies. Precise measurements of the low-energy γ rays emitted following thermal-neutron capture have been previously made by Gruber[1] and Melioranskii, Kalinkin, and Estulin (MKE).[2] Using these data together with the Ritz combination principle, MKE have reconstructed the level diagram for the low-lying states in Rh^{104}.

The number of low-energy γ rays that have been observed is very large. Schult[3] observed 255 γ rays in the energy range 32.22 to 406.31 keV, with an average spacing of 1.66 keV. This leads to a large probability of accidental combinations. Thus, the direct observation of the levels, through (d,p) or high-energy (n,γ) measurements, forms the best way for identifying and verifying the existence of low-lying states.

The high-energy γ-ray spectrum of thermal-neutron capture has been investigated previously.[4-6] Thermal-neutron capture in Rh^{103}, however, is completely dominated by the 1.257-eV resonance. Since resonance-capture γ spectra display large fluctuations in intensity, the study of the γ spectra of the resonance capture in a number of resonances is necessary for the observation of a more detailed structure in Rh^{104}.

II. EXPERIMENTAL CONDITIONS

These measurements were performed at the fast chopper facility[7] of the high flux beam reactor of Brookhaven National Laboratory. A sample of 198 g of natural rhodium ($Z = 45$, $A = 103$) in powdered form, wrapped in a thin aluminum foil, was used as the capturing sample. This was placed in the neutron beam at the 22-m station at an angle of 45° to the direction of the beam as shown in Fig. 1(a). The sample was viewed by a 4-cm^3 Ge(Li) planar diode detector which was placed outside the collimated neutron beam. Standard low-noise preamplifiers, amplifiers, and a 2048-channel pulse-height digitizer were used for these measurements. The detector was shielded with both Li^6 and wax in order to reduce the probability of scattered neutron capture in the detector and its associated structural supports. The over-all resolution of the detector was observed to be 6 keV for a γ-ray energy of about 7.3 MeV.

The events were recorded in digital form on magnetic tape, from which the desired spectra were later assembled.

In order to cover the neutron energy range from thermal to over 200 eV with adequate resolution and neutron intensity, two chopper speeds were used. A group of four runs was taken using a chopper speed of 3000 rpm with timing channels 4 μsec wide and covering a neutron energy range $0.15 < E_n < 30$ eV. A second group of six runs was taken with a chopper speed of 10 000 rpm and timing channels 1 μsec wide in which neutrons of energy $19 < E_n < 907$ eV were covered. Supplementary data at higher neutron energies were recorded at the 48.8-m flight station, taking advantage of the annular sample geometry shown in Fig. 1(b). The high solid

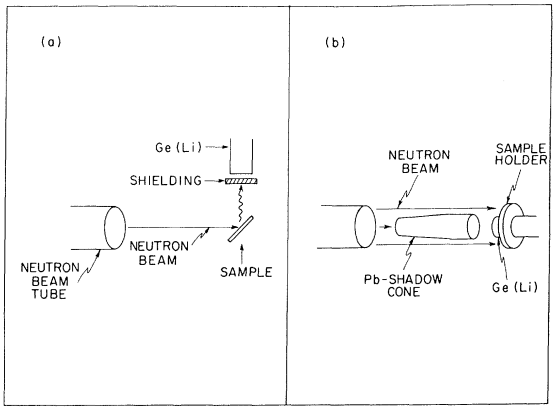

FIG. 1. Experimental arrangement showing the geometry of the sample and the detector. (a) Regular geometry. (b) Annular geometry.

angle afforded by this geometry compensates for the lower beam intensity at this flight path.

The γ-ray spectrum was obtained for γ rays which deposit energies within the range from 2.998 to 6.854 MeV at a gain of 2.046-keV per channel.

Four more tapes were recorded at the 3000-rpm chopper speed, with a mixed target of rhodium and chromium in the beam. These runs were used for calibrating the γ-ray energies.

A run was also taken with a carbon scatterer in the beam at a chopper speed of 10 000 rpm and was used to estimate the background contribution to the continuum.

The over-all continuous running time of the experiment was three weeks.

III. DATA REDUCTION

The time-of-flight spectrum obtained for the resonance-neutron capture in rhodium at 22-m flight path is shown in Fig. 2(a). As seen in the figure, three resonances are completely resolved. These are the previously determined[8] p-wave resonances at 34.4 eV and the two s-wave resonances at 46.7 and 68.3 eV. Four more s-wave resonances are seen to be adequately resolved from one another. These are the resonances at 95.6, 125.5, 154.2, and 187.0 eV. These are not, however, resolved from neighboring weak p-wave resonances. Because of the smaller neutron widths for p-wave levels, the contribution to the γ-ray spectra from these resonances is expected to be very small compared with the contribution of the s-wave resonances. Thus the observed spectra in the overlapping region is mainly due to the s-wave levels, which are adequately resolved. The limits for which γ-ray spectra were obtained are indicated in Fig. 2 by the brackets underneath the peaks. The scan over the peak at the high-energy end of the neutron time-of-flight spectrum corresponds to captured

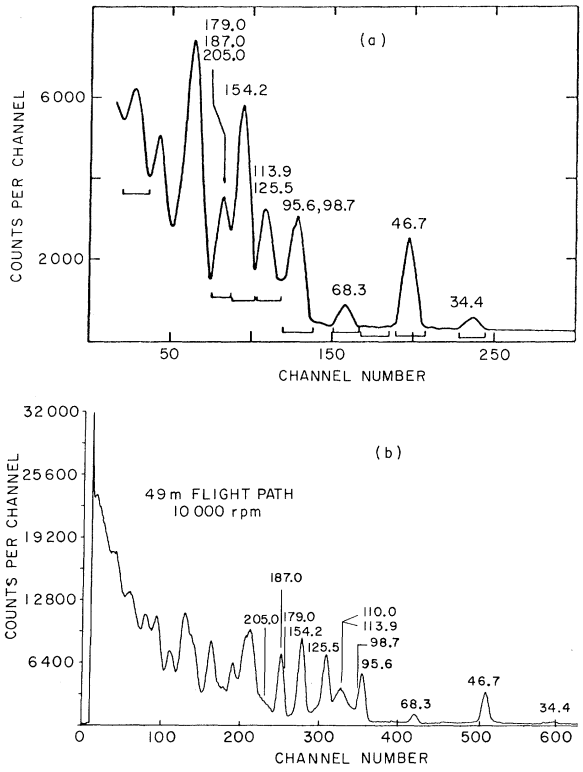

FIG. 2. Neutron time-of-flight spectra for rhodium. (a) Regular geometry (upper figure). (b) Annular geometry (lower figure). The effect of neutron capture in the germanium detetector is displayed in the broad background peak near 100 eV. This is associated with a resonance in Ge^{73} at 102 eV.

neutrons of energies from 530 to 900 eV. This range includes 16 resonances, seven of which are known to be $l=0$ resonances, six have $l=1$, while the l values for the remaining three are not known.

The neutron energy range covered by the low-energy run (3000 rpm) includes only the s-wave resonance at 1.257 eV. Although the low-energy cutoff in this run is 0.15 eV, the low-energy end of the neutron spectrum ($0.15 < E_n < 0.49$ eV) was taken as equivalent to a thermal-capture run. This is justifiable, since the thermal capture is completely dominated by the 1.257-eV resonance.

The γ-ray spectrum obtained following thermal capture is shown in Fig. 3. The energy and relative intensity for a γ ray were obtained from the respective double-escape peak position and area using the peak-fitting program as described elsewhere.[9] The energy scale was calibrated using the chromium lines 7100.2 and 6644.5 keV which were measured by Kane and Mariscotti[10] from the Cr^{53}-$(n,\gamma)Cr^{54}$ reaction. Pulses from a highly stable pulser were used to correct for the system nonlinearity over the energy range covered in the experiment.

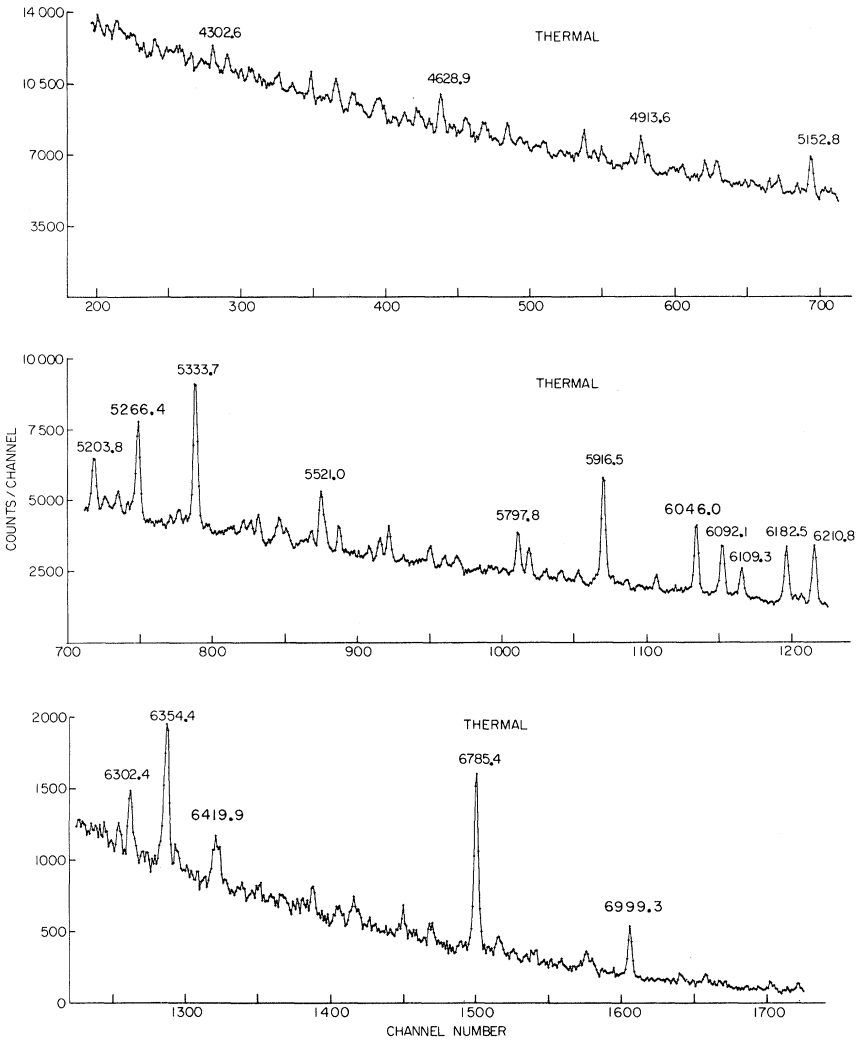

FIG. 3. γ-ray spectra for thermal-neutron capture in rhodium.

The intensities were normalized to absolute values by comparison with the absolute intensities of Rasmussen *et al.*[5] for thermal-capture γ rays. The energies and intensities obtained in this experiment are listed in Table I. The errors in energy include only the uncertainty in the peak position and do not include the uncertainty in the absolute energy scale, which is believed to be 1.5 keV.

A value of 6999.3 ± 0.2 keV for the ground-state transition in Rh^{104} was obtained in this experiment. This is in very good agreement with the values obtained in other independent measurements. A value of 6999 ± 3 keV was measured by Hughes, Kennett, and Prestwich (HKP).[6] No systematic differences with energy are seen in comparison with either Refs. 5 or 6.

Since the γ-ray intensities were normalized to those of Rasmussen *et al.*,[5] the agreement between the two measurements is good, as would be expected. The absolute values reported by HKP[6] are about a factor of 2 larger than what we obtained. However, the relative intensities are in better agreement.

The list of Table I includes 119 transitions with energies greater than 4135 keV which were not reported previously. This is due to the fact that the existence of many transitions was exhibited from resonance-capture spectra and due to the improvement of the resolution over the other measurements.

The γ-ray spectra following capture in the individual resonances are shown in Figs. 4 and 5. The γ-ray intensities following resonance capture were normalized to absolute values using the thermal run after correcting for the background contributions to the spectra. The carbon run was used to

TABLE I. Energies and intensities of γ rays emitted in thermal-neutron capture in rhodium, and in broad epithermal-neutron energy ranges for the reaction $Rh^{103}(n,\gamma)Rh^{104}$.

E_γ (keV)	ΔE (keV)	$0.14 < E_n < 0.487$ eV I (No./1000)	ΔI (No./1000)	$0.14 < E_n < 15$ eV I (No./1000)	ΔI (No./1000)	$2.2 < E_n < 900$ eV I (No./1000)	ΔI (No./1000)
6999.3	0.2	1.76	0.11	1.63	0.06	1.83	0.06
6948.0	0.3	0.30	0.11	0.51	0.05	0.92	0.08
6902.3	0.6	0.19	0.12	0.33	0.05	1.48	0.10
6820.2	0.4	0.24	0.11	0.24	0.05	1.30	0.11
6814.3	0.3	0.44	0.10	0.49	0.06	0.79	0.09
6801.9	1.0	0.13	0.11	0.39	0.07	0.51	0.10
6785.6	0.1	4.75	0.14	5.40	0.12	7.45	0.11
6768.0	0.8	−0.01	0.09	0.24	0.06	0.43	0.07
6762.6	0.6	0.26	0.09	0.32	0.05	0.27	0.12
6753.4	0.8	0.06	0.11	0.07	0.07	0.41	0.08
6731.3	0.5	0.04	0.12	0.00	0.11	0.51	0.11
6726.6	1.0	0.30	0.19	0.33	0.11	0.13	0.11
6657.5	1.1	0.18	0.12	0.20	0.06	0.25	0.10
6615.3	0.3	0.88	0.11	0.67	0.07	1.08	0.10
6576.8	0.5	0.00	0.13	0.09	0.12	1.10	0.18
6514.5	0.3	0.52	0.09	0.46	0.05	2.66	0.30
6484.0	0.4	0.48	0.14	0.27	0.14	0.64	0.06
6476.6	0.3	0.36	0.30	0.28	0.07	0.95	0.07
6459.6	0.3	0.24	0.16	0.40	0.06	2.21	0.13
6419.9	0.3	1.09	0.14	1.19	0.08	2.41	0.12
6413.5	1.5	0.12	0.15	0.31	0.14	0.93	0.13
6406.9	0.5	0.25	0.11	0.37	0.07	0.67	0.11
6397.1	0.8	0.10	0.12	0.36	0.07	0.61	0.13
6379.7	0.7	0.14	0.13	0.43	0.07	0.68	0.14
6354.4	0.3	4.54	0.15	4.11	0.17	3.03	0.18
6302.4	0.2	1.88	0.15	1.77	0.07	1.30	0.12
6287.1	0.2	0.00	0.13	0.90	0.17	1.71	0.18
6210.8	0.2	8.02	0.18	7.41	0.20	3.66	0.24
6206.5	0.3	0.47	0.17	1.20	0.18	1.37	0.23
6193.2	0.3	1.30	0.17	1.60	0.11	1.27	0.19
6182.5	0.3	0.73	0.17	1.37	0.12	1.95	0.19
6171.8	0.1	6.82	0.24	6.90	0.31	5.10	0.23
6163.9	0.5	0.59	0.22	0.97	0.26	1.92	0.20
6133.5	0.2	0.15	0.20	0.67	0.08	3.22	0.53
6109.2	0.1	2.63	0.11	3.86	0.09	5.57	0.17
6100.6	0.3	0.07	0.11	0.83	0.08	1.02	0.13
6092.1	0.9	0.03	0.17	0.77	0.08	1.23	0.16
6082.8	0.1	5.83	0.20	6.40	0.13	6.38	0.19
6067.4	0.5	0.15	0.17	0.72	0.09	0.83	0.17
6056.3	0.8	−0.09	0.21	0.50	0.13	1.32	0.21
6046.0	0.1	8.46	0.22	8.22	0.15	4.78	0.23
6026.0	0.3	0.15	0.19	0.45	0.09	1.61	0.14
6017.0	0.4	0.18	0.19	0.39	0.09	1.52	0.14
6011.3	0.6	0.13	0.14	0.51	0.09	0.82	0.15
5989.8	0.2	1.38	0.13	1.84	0.09	2.83	0.48
5966.6	0.4	0.39	0.16	0.70	0.11	0.93	0.16
5948.6	0.2	0.86	0.21	1.06	0.09		
5934.9		0.54	0.23	0.44	0.09	1.00	0.18
5927.1	0.4	1.11	0.28	1.06	0.15	2.05	0.16
5916.5	0.0	12.85	0.29	11.92	0.19	6.48	0.18
5906.5	0.4	1.30	0.25	1.81	0.35	1.58	0.16
5880.9	0.2	1.18	0.12	1.33	0.10	0.95	0.14
5847.7	0.4	0.02	0.20	0.49	0.11	1.28	0.13
5836.5	0.8	0.54	0.22	0.96	0.22	1.13	0.14
5820.4	0.7	0.00	0.20	0.25	0.16	0.58	0.10
5812.2	0.3	3.48	0.13	3.35	0.12	2.05	0.11
5803.4	0.7	0.26	0.14	0.20	0.14	0.64	0.11

TABLE I *(Continued)*

E_γ (keV)	ΔE (keV)	$0.14 < E_n < 0.487$ eV ΔI (No./1000)	I (No./1000)	$0.14 < E_n < 15$ eV I (No./1000)	ΔI (No./1000)	$2.2 < E_n < 900$ eV I (No./1000)	ΔI (No./1000)
5797.8	0.2	5.21	0.15	4.84	0.10	2.75	0.11
5786.8	1.0	0.25	0.13	0.37	0.16	0.91	0.11
5766.6	0.4	0.61	0.19	0.88	0.10	1.29	0.14
5757.7	0.4	0.86	0.20	0.94	0.10	0.75	0.15
5743.0	0.3	0.33	0.14	0.67	0.10	0.88	0.11
5734.0	0.3	−0.06	0.14	0.35	0.10	0.91	0.11
5713.5	0.5	0.37	0.20	0.78	0.14	1.55	0.21
5708.4	0.8	1.42	0.20	1.12	0.22	2.17	0.23
5695.1	0.4	1.11	0.14	1.35	0.11	1.65	0.25
5688.8	0.9	−0.16	0.16	0.56	0.11	1.25	0.24
5674.1	0.2	1.61	0.19	2.55	0.18	1.25	0.23
5656.0	1.0	0.37	0.13	0.52	0.11	0.71	0.18
5648.3	1.0	0.01	0.14	0.33	0.11	1.21	0.11
5634.4	0.4	0.48	0.10	0.79	0.13	1.13	0.14
5616.5	0.2	2.89	0.21	3.35	0.11	1.79	0.13
5604.4	0.3	1.27	0.28	2.55	0.16	1.98	0.14
5587.9	0.3	0.63	0.16	1.24	0.13	1.68	0.15
5574.8	0.6	0.00	0.22	0.25	0.11	0.79	0.14
5566.1	0.6	0.06	0.22	0.35	0.13	0.69	0.15
5546.6	0.2	2.44	0.20	2.82	0.13	1.37	0.15
5527.0	0.3	1.69	0.24	2.36	0.22	2.22	0.18
5521.0	0.2	5.16	0.25	5.61	0.23	2.57	0.18
5507.6	0.2	1.33	0.23	2.02	0.15	1.13	0.14
5493.6	0.5	0.19	0.24	0.85	0.16	0.75	0.14
5476.2	0.6	0.12	0.17	0.63	0.16	1.29	0.11
5472.5	0.4	1.25	0.13	1.77	0.14	0.97	0.14
5463.3	0.3	1.98	0.23	2.76	0.16	1.71	0.11
5456.8	0.6	0.78	0.22	0.75	0.16	0.27	0.17
5453.3	0.7	−0.19	0.20	0.49	0.17	0.70	0.11
5441.4	0.7	0.00	0.17	0.60	0.18	0.59	0.14
5434.5	0.3	2.79	0.20	2.41	0.14	1.51	0.13
5422.9	0.2	1.66	0.16	2.14	0.11	1.52	0.13
5413.5	0.3	1.59	0.17	1.99	0.12	1.50	0.13
5399.2	0.6	0.46	0.18	1.19	0.15	1.02	0.19
5391.5	0.7	0.65	0.17	0.89	0.13	1.00	0.24
5364.5	0.4	0.21	0.28	1.65	0.51	1.52	0.15
5354.9	0.5	0.68	0.24	1.64	0.22	1.39	0.14
5346.5	0.2	14.48	0.29	13.99	0.22	8.32	0.62
5333.7	0.9	0.71	0.25	2.46	0.33	0.99	0.14
5323.0	0.4	1.99	0.18	2.23	0.19	1.44	0.13
5311.5	0.4	0.70	0.17	1.26	0.18	0.97	0.12
5298.0	0.7	0.39	0.17	0.72	0.18	0.71	0.12
5266.4	0.1	9.06	0.30	8.82	0.15	4.18	0.19
5257.3	0.6	1.15	0.26	1.69	0.13	1.76	0.19
5251.0	0.4	1.19	0.26	1.53	0.13	0.93	0.19
5237.7	0.2	2.04	0.15	2.41	0.11	2.28	0.22
5223.1	0.5	1.03	0.15	1.20	0.11	1.47	0.18
5217.6	0.4	1.13	0.16	1.44	0.12	1.28	0.19
5203.8	0.2	5.22	0.23	4.83	0.23	2.08	0.33
5186.8	0.6	0.44	0.35	0.85	0.14	0.59	0.13
5180.2	0.6	1.04	0.34	1.29	0.14	0.98	0.17
5173.1	0.7	1.09	0.35	1.23	0.25	1.21	0.18
5152.8	0.2	5.68	0.29	4.81	0.27	2.49	0.25
5142.9	0.4	0.95	0.24	1.19	0.12	0.77	0.25
5133.6	0.3	1.20	0.19	1.57	0.12	0.98	0.24
5123.4	0.5	0.02	0.20	0.44	0.12	0.69	0.26
5106.9	0.4	1.57	0.41	1.99	0.22	1.52	0.21
5094.0	0.3	1.30	0.42	1.46	0.17	1.18	0.15

TABLE I *(Continued)*

E_γ (keV)	ΔE (keV)	$0.14 < E_n < 0.487$ eV I (No./1000)	ΔI (No./1000)	$0.14 < E_n < 15$ eV I (No./1000)	ΔI (No./1000)	$2.2 < E_n < 900$ eV I (No./1000)	ΔI (No./1000)
5082.2	0.5	0.88	0.20	0.43	0.13	1.21	0.20
5070.0	0.4	1.00	0.21	1.28	0.13	1.15	0.21
5060.2	0.3	0.80	0.32	1.08	0.12	0.83	0.22
5036.9	0.7	0.37	0.29	0.45	0.12	0.56	0.13
5031.4	0.6	0.52	0.21	0.57	0.12	0.56	0.13
5020.9	0.3	2.76	0.33	2.46	0.26	1.58	0.14
5004.3	0.3	2.32	0.32	2.56	0.13	1.50	0.12
4978.3	0.8	0.86	0.21	0.16	0.12	1.13	0.21
4972.7	0.5	1.08	0.23	1.70	0.18	1.35	0.20
4960.8	0.6	1.25	0.19	1.10	0.19	1.18	0.23
4950.0	1.2	0.18	0.29	0.68	0.21	0.79	0.23
4923.0	0.6	2.27	0.21	2.45	0.38	1.61	0.25
4913.6	0.3	4.04	0.20	4.54	0.26	2.74	0.25
4900.6	0.3	2.46	0.23	2.19	0.26	1.64	0.24
4890.8	0.6	0.18	0.29	1.09	0.29	1.03	0.28
4863.2	1.1	0.57	0.40	0.85	0.12	0.74	0.17
4858.2	0.9	2.02	0.35	1.70	0.21	0.88	0.21
4848.2	0.4	1.59	0.27	1.77	0.19	1.21	0.17
4838.7	0.8	0.31	0.26	0.76	0.18	0.79	0.12
4834.1	0.2	3.84	0.26	3.93	0.18	1.77	0.12
4824.3	0.5	0.90	0.26	1.18	0.18	0.90	0.12
4811.8	0.8	0.56	0.22	1.54	0.19	1.09	0.21
4800.6	0.6	0.92	0.22	1.17	0.15	1.79	0.32
4778.6	0.6	0.79	0.28	1.13	0.14	0.99	0.42
4773.4	0.7	0.80	0.27	1.80	0.27	0.96	0.24
4765.5	0.5	0.86	0.34	1.25	0.24	1.07	0.19
4751.1	0.6	1.31	0.23	1.39	0.20	1.19	0.33
4743.3	0.5	1.47	0.24	1.94	0.21	1.00	0.25
4735.2	0.8	0.00	0.31	1.10	0.19	1.02	0.25
4724.9	0.3	2.73	0.32	3.17	0.19	1.80	0.21
4709.3	0.5	0.46	0.36	1.00	0.12	0.81	0.23
4697.4	0.6	1.40	0.36	1.69	0.27	1.08	0.16
4690.4	0.4	2.12	0.35	2.47	0.26	2.45	0.38
4671.0	0.5	1.39	0.30	1.53	0.35	1.30	0.21
4665.0	0.5	2.05	0.31	2.37	0.38	1.16	0.20
4649.2	0.6	0.73	0.38	1.25	0.18	0.81	0.24
4642.9	0.8	0.75	0.46	1.10	0.20	1.28	0.20
4628.9	0.6	5.26	0.51	6.16	0.39	1.72	0.20
4614.2	0.5	1.05	0.27	1.50	0.18	1.01	0.17
4601.9	0.9	1.17	0.22	2.28	0.64	1.08	0.21
4595.1	0.6	1.68	0.21	2.07	0.46	1.80	0.21
4586.8	0.4	0.44	0.20	0.88	0.12	0.74	0.17
4579.5	0.3	1.66	0.37	1.58	0.12	1.11	0.15
4568.1	0.9	0.25	0.45	0.76	0.51	1.51	0.15
4563.0	0.9	0.45	0.45	0.50	0.52	1.36	0.17
4549.3	0.7	1.05	0.40	1.66	0.24	1.43	0.35
4542.8	0.6	2.24	0.40	2.64	0.24	0.99	0.31
4536.4	0.6	1.58	0.39	1.92	0.24	1.36	0.32
4522.2	1.0	0.42	0.58	0.69	0.15	0.43	0.19
4515.4	0.4	1.29	0.46	1.50	0.18	0.48	0.20
4502.2	0.4	1.65	0.49	1.85	0.16	0.65	0.26
4483.9	0.4	0.96	0.42	2.11	0.22	1.30	0.14
4478.7	0.3	3.15	0.34	2.99	0.22	1.91	0.13
4455.9	0.6	0.55	0.28	0.97	0.13	0.58	0.13
4444.6	0.2	2.94	0.25	3.14	0.20	1.68	0.15
4429.1	0.6	0.35	0.37	1.09	0.17	0.00	0.27
4417.7	0.3	0.35	0.37	1.60	0.13	0.79	0.15
4407.7	0.4	−0.28	0.33	0.76	0.13	1.09	0.25

TABLE I *(Continued)*

E_γ (keV)	ΔE (keV)	$0.14 < E_n < 0.487$ eV I (No./1000)	ΔI (No./1000)	$0.14 < E_n < 15$ eV I (No./1000)	ΔI (No./1000)	$2.2 < E_n < 900$ eV I (No./1000)	ΔI (No./1000)
4398.1	0.3	1.50	0.31	2.23	0.16	1.79	0.26
4392.0	0.6	0.64	0.31	1.44	0.16	0.93	0.27
4384.2	0.6	0.07	0.32	0.98	0.13	0.11	0.24
4377.4	0.5	0.06	0.32	0.94	0.20	0.87	0.28
4368.7	0.9	0.24	0.29	1.36	0.18	0.73	0.27
4360.3	0.5	1.28	0.30	1.80	0.24	1.02	0.28
4354.3	0.3	1.73	0.32	1.67	0.26	0.87	0.22
4343.5	0.4	1.04	0.21	1.63	0.13	0.50	0.19
4334.9	0.4	0.68	0.23	1.36	0.13	0.45	0.17
4326.9	0.6	1.33	0.37	1.38	0.20	0.72	0.22
4321.8	0.3	1.39	0.41	2.59	0.21	0.60	0.21
4310.1	0.5	0.14	0.32	1.25	0.19	0.67	0.18
4302.6	0.2	2.74	0.31	3.39	0.18	1.28	0.17
4294.5	0.5	0.94	0.29	1.33	0.19	0.35	0.26
4287.9	0.8	0.00	0.40	1.54	0.20	0.44	0.16
4282.9	0.7	0.82	0.54	0.61	0.21	0.89	0.16
4270.2	0.5	0.76	0.40	1.77	0.32	0.97	0.27
4256.8	0.4	1.26	0.38	2.25	0.24	1.45	0.26
4248.8	0.5	1.43	0.36	2.18	0.24	0.60	0.17
4241.9	0.9	0.54	0.37	1.64	0.24	0.62	0.17
4233.9	0.5	1.12	0.39	1.69	0.24	0.98	0.28
4222.6	0.6	0.44	0.37	1.21	0.17	0.20	0.20
4216.2	0.4	0.91	0.36	2.29	0.16	1.07	0.28
4198.8	0.8	0.10	0.35	1.09	0.21	0.45	0.29
4187.2	1.0	0.56	0.34	1.39	0.36	0.90	0.27
4181.4	1.5	0.87	0.35	1.53	0.33	0.34	0.13
4171.6	0.8	0.09	0.38	1.34	0.22	1.45	0.32
4165.3	0.8	1.16	0.38	1.50	0.21	0.46	0.13
4158.6	0.4	1.47	0.36	2.46	0.19	0.33	0.27
4146.3	0.6	0.00	0.43	1.46	0.19	0.35	0.30
4132.1	0.4	1.10	0.35	1.77	0.17	0.37	0.33

determine these background contributions.

The γ-ray intensities obtained for neutron capture in the different resonances for 145 final states are listed in Table II. These intensities reflect the wide fluctuations generally observed in resonance-capture spectra. Since thermal capture is dominated by one resonance, these fluctuations show the importance of the capture study in other resonances in obtaining information about final states in Rh^{104}.

IV. CAPTURING STATES

The ground state of Rh^{103} is a $\frac{1}{2}^-$ state, thus capture of an s-wave neutron leads to states with spin 0^- or 1^-. On the other hand, p-wave capture will lead to the formation of states with spin 0^+, 1^+, or 2^+. Intensities from neutron capture in the 34.4-eV p-wave resonance could not be determined, because of the lack of sufficient statistics which could give meaningful results. The strongest transition in the spectrum of this resonance has an energy of 6407 keV, as shown in Fig. 6. The intensity of this transition is estimated to be about 10 photons per 1000 neutron capture in the resonance. Of the s-wave resonances studied in this experiment, the 46.7-, 95.6-, and 154.2-eV resonances had all been assigned[8] a spin 0^-, while the resonances at 1.257, 125.5, and 187.0 eV had been assigned[8] as 1^-. No previous spin assignment had been made for the s-wave resonance at 68.3 eV. Although, in general, a spin assignment to a resonance level can be made by observing its decay to low-lying states, such an assignment was not possible for this resonance owing to the fact that only one of the transitions proceeding from this level populates a final state with a unique spin assignment. This is the transition to the 1^+ ground state, which can be populated via an $E1$ transition from either spin 0^- or 1^-.

A relatively strong transition (~0.5 the single-particle estimate for $E1$ transitions) with energy 6902 keV is observed in the spectrum of the 95.6-eV resonance. This transition, which is not observed for thermal neutrons, populates the second

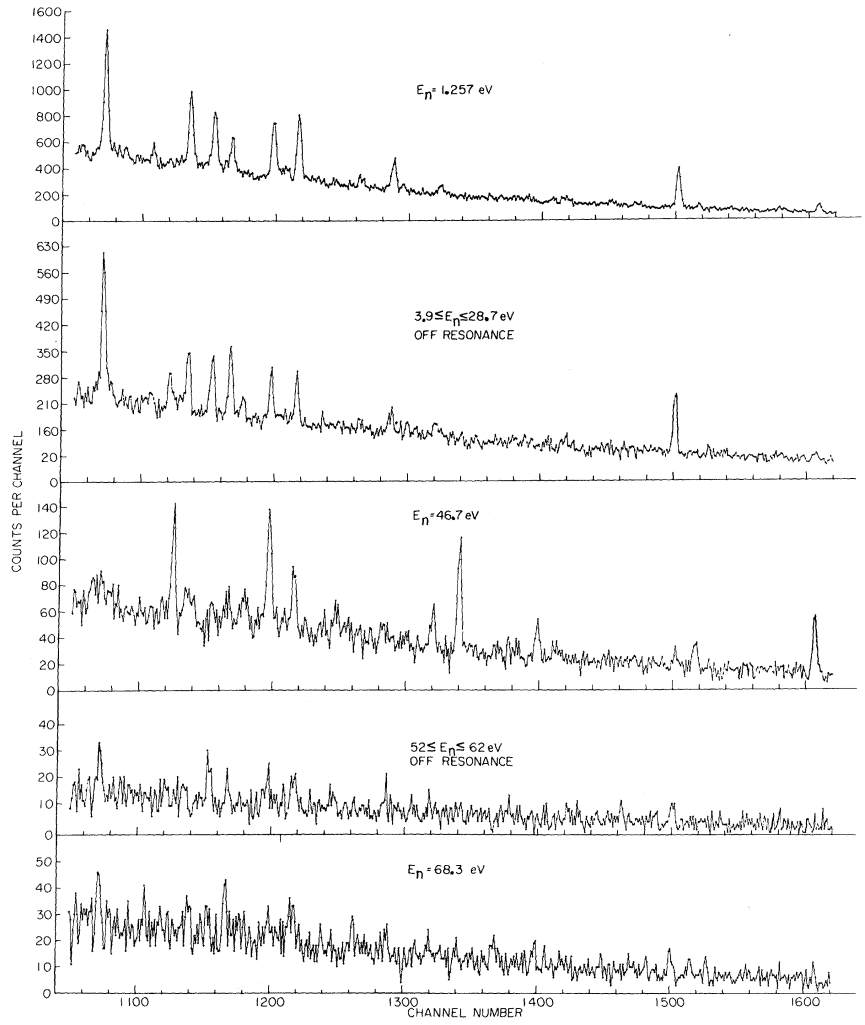

FIG. 4. γ-ray spectra for resonance-neutron capture in rhodium.

excited state at 97 keV. This state has been determined to have a spin of 2^+ by Greenwood[11] from the decay of the 5^+ isomeric state at 129 keV. The 95.6-eV resonance has been assigned a spin of 0^- by Trochon, Lottin, and Rubin[12] and independently by Wang *et al.*[13] from transmission and scattering measurements. The only possible transition connecting such initial and final states will give rise to $M2$ radiation. Since $M2$ transitions have never been observed in high-energy γ-ray transitions, this implies that if the spin assignment of 2^+ for the 97-keV state is assumed certain, the 95.6-eV resonance should have a spin of 1^- and not 0^-. This agrees with the tentative assignment of Moxon and Rae (see Ref. 2).

In order to ascertain that this transition arises from neutron capture in the 95.6-eV resonance and not in the p-wave resonance at 98.7 eV, an additional run was taken with a flight path of 48.9 m with an annular geometry as shown in Fig. 1(b). Scans over the energy regions corresponding to the positions of the unresolved 95.6- and 98.7-eV resonances showed conclusively that the above-mentioned transition belongs to the 95.6-eV resonance.

V. LOW-LYING STATES

Level diagrams for Rh^{104}, as determined from low-energy γ rays and electron-conversion measurements, are given in the compilation of Bartholomew *et al.*[14]

While transitions from a capturing state of spin 1^- can proceed to a final state of spin 0^+, 1^+, or 2^+ by $E1$ radiation, only states of spin 1^+ can be populated by $E1$ transitions from 0^- capture levels. Thus, it is possible to identify the 1^+ low-lying states whenever they are populated strongly following capture in 0^- resonances. Furthermore, since only high-energy transitions of $E1$, $M1$, or $E2$ multipolarity are observed experimentally, only final states of spin 1^+, 1^-, or 2^- can be populated from the decay of the 0^- levels. One, however, should

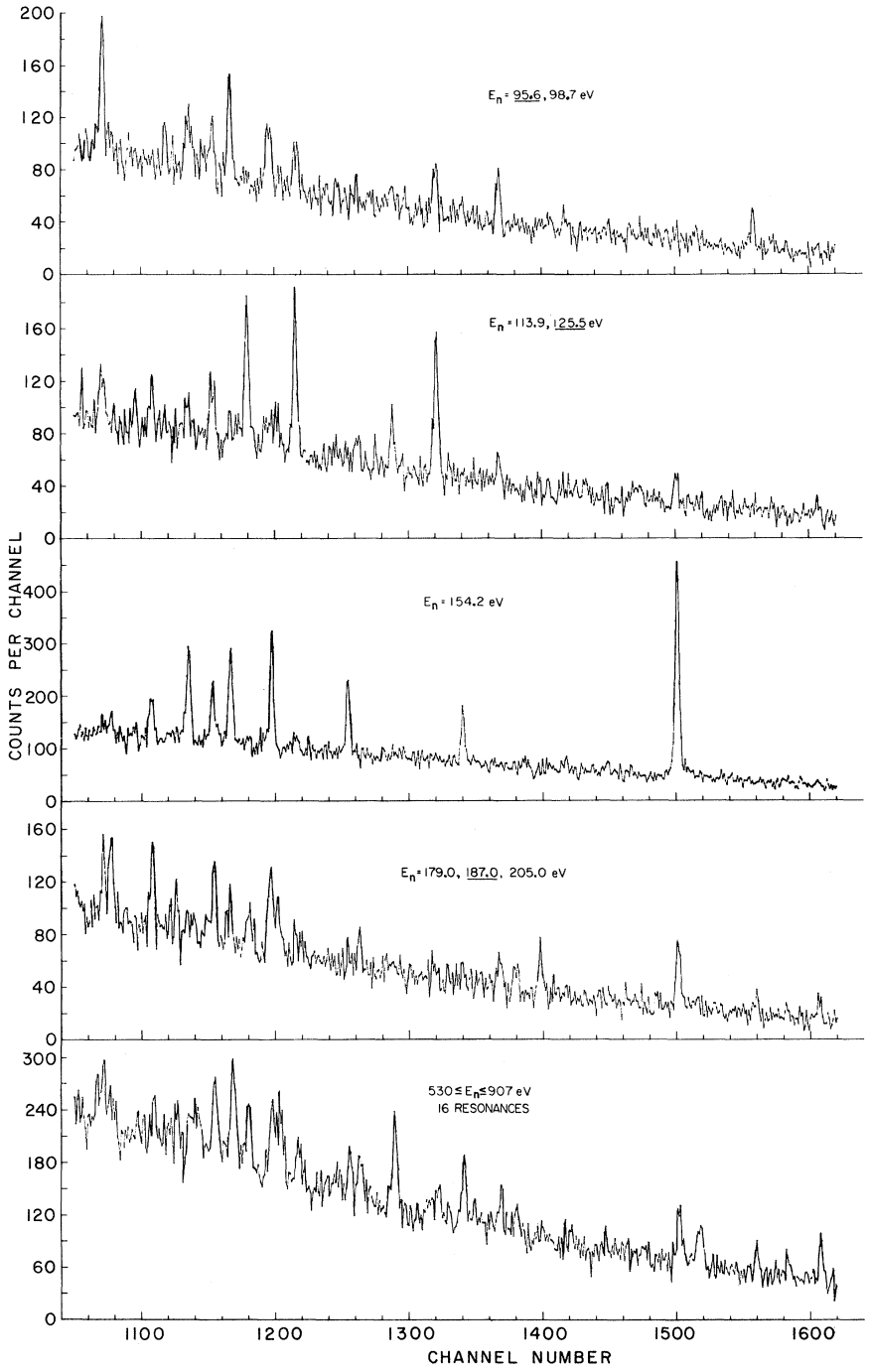

FIG. 5. γ-ray spectra for resonance-neutron capture in rhodium.

be careful when applying these restrictions to the weak transitions observed in this experiment, since no correction has been made for the contribution of adjacent overlapping 1^- levels nor for the possible contributions from capture in the unresolved p-wave levels.

The final states below 700 keV to which transitions are observed in this experiment are shown in Fig. 7. The spins indicated are those obtained from the observed high-energy transitions using the arguments presented above, coupled with the assignments based on previous work cited in Ref. 14. A comparison of Fig. 7 with Ref. 14 shows that of the 29 levels previously observed below 645 keV, 13 are populated by high-energy γ-ray transitions. A close doublet at 266.8 and 269.3 keV and the doublet at 524.5 and 524.7 keV, assigned from the low-energy γ-ray spectra, are seen as a single state

TABLE II. Energies and intensities of γ rays observed in the resonance-neutron capture in rhodium for the reaction $Rh^{103}(n,\gamma)Rh^{104}$. Intensities are expressed in photons per 1000 captures.

E_γ	$E_n = 1.257$ eV		$E_n = 46.7$ eV		$E_n = 68.3$ eV		$E_n = 95.6$ eV		$E_n = 125.5$ eV		$E_n = 154.2$ eV		$E_n = 187.0$ eV		$530 < E_n < 907$ eV	
(keV)	I	ΔI	I	ΔI	I	ΔI	I	ΔI	I	ΔI	I	ΔI	I	ΔI	I	ΔI
6999.3	1.38	0.11	9.07	0.81	1.74	0.94	2.08	0.63	2.46	0.67	1.76	0.42	2.28	0.45	3.53	0.28
6948.0	0.43	0.08	1.21	0.42	1.00	1.06	0.63	0.51	1.47	0.56	1.61	0.59	1.06	0.30	1.62	0.41
6902.3	0.19	0.08	0.85	0.56	0.77	1.09	5.47	0.75	1.74	0.52	0.49	0.32	2.02	0.48	2.17	0.34
6820.2	0.37	0.18	1.93	0.55	0.40	0.68	0.27	0.49	1.29	0.62	1.84	0.61	0.03	0.54	2.78	0.44
6814.3	0.33	0.18	3.31	0.60	1.65	0.74	2.27	0.57	0.42	0.67	−0.03	0.63	0.83	0.61	2.12	0.44
6801.9	0.27	0.16	−0.21	0.43	0.00	1.03	0.26	0.78	1.64	0.70	1.84	0.50	0.79	0.53	0.41	0.50
6785.6	5.81	0.21	2.61	0.43	4.55	1.36	1.81	0.70	5.12	0.73	45.38	0.92	7.39	0.54	4.61	0.56
6768.0	0.36	0.14	0.87	0.42	0.00	1.03	2.14	0.75	0.11	0.57	1.68	0.42	0.58	0.60	0.89	0.75
6762.6	0.24	0.11	0.76	0.40	0.66	1.11	0.63	0.90	0.54	0.72	0.46	0.53	0.00	0.54	0.35	0.57
6753.4	0.00	0.17	1.15	0.40	0.00	1.11	1.96	0.72	0.83	0.86	0.56	0.66	2.30	0.57	0.23	0.31
6731.3	0.35	0.15	0.00	0.29	0.00	1.12	0.00	0.65	2.36	0.54	0.00	0.53	0.77	0.56	0.48	0.37
6726.6	0.45	0.11	1.01	0.49	1.27	1.24	1.33	0.61	1.58	0.43	0.53	0.46	0.16	0.45	0.00	0.37
6657.5	0.30	0.10	0.53	0.56	0.00	1.14	1.30	0.60	0.00	0.78	1.82	0.50	0.32	0.34	0.33	0.42
6615.3	0.76	0.17	1.93	0.55	1.00	1.12	2.59	0.51	2.07	0.83	2.18	0.67	1.20	0.86	0.74	0.45
6576.8	−0.04	0.13	5.31	0.69	2.70	1.24	1.27	0.49	1.20	0.87	0.21	0.51	4.53	0.49	1.46	0.49
6514.5	0.42	0.16	1.47	0.52	2.42	1.45	6.77	0.76	4.86	0.75	1.49	0.66	2.74	0.73	4.01	0.97
6484.0	0.20	0.14	1.11	0.52	0.71	1.42	0.87	0.63	1.66	0.70	0.95	0.38	1.34	0.53	0.86	0.45
6476.6	0.08	0.14	0.85	0.56	0.00	1.18	0.97	0.79	1.64	0.89	1.63	0.40	−0.03	0.53	1.62	0.49
6459.6	0.14	0.18	14.74	1.01	1.54	1.42	3.33	0.81	1.62	0.99	9.86	0.63	1.69	0.58	4.60	0.42
6419.9	0.76	0.19	5.51	0.81	1.90	1.23	6.16	1.11	17.97	1.15	1.66	0.50	1.54	0.60	2.64	0.42
6413.5	0.00	0.18	1.15	0.59	0.66	1.18	2.51	1.30	1.58	0.87	0.00	0.64	1.73	0.60	0.89	0.59
6406.9	0.19	0.19	0.64	0.70	0.00	1.18	0.60	0.87	1.01	0.83	0.77	0.51	−0.01	0.61	1.54	0.38
6397.1	0.23	0.16	0.90	0.60	0.81	1.39	1.48	0.57	0.42	0.77	0.74	0.71	0.58	0.48	−0.04	0.40
6379.7	0.25	0.14	1.92	0.59	0.00	1.15	−0.19	0.55	0.59	0.66	0.68	0.60	0.85	0.42	0.06	0.35
6354.4	3.80	0.23	1.62	0.64	2.94	1.51	3.20	0.69	6.78	0.63	1.60	0.42	1.24	0.46	6.36	0.50
6302.4	0.90	0.22	0.95	0.76	3.37	1.56	2.35	0.76	3.76	0.86	1.04	0.56	3.57	0.71	2.18	0.48
6287.1	0.35	0.22	2.54	0.77	0.00	1.27	0.27	0.69	1.67	0.77	12.24	0.71	1.27	0.49	3.07	1.38
6210.8	7.61	0.25	9.12	0.76	4.30	1.39	3.80	0.70	1.99	0.78	2.45	0.74	2.46	0.64	2.51	0.40
6206.5	0.50	0.29	0.64	0.70	4.28	1.33	3.29	0.72	16.85	0.89	0.15	0.79	1.89	0.74	0.25	0.57
6193.2	1.75	0.17	2.86	0.76	1.83	1.55	1.36	0.65	0.75	1.08	0.57	0.78	0.46	0.53	0.57	0.57
6182.5	1.26	0.17	2.30	0.73	2.04	1.54	2.18	0.61	4.50	1.10	−0.12	0.74	4.50	0.57	4.46	0.59
6171.8	6.85	0.24	15.60	0.97	3.41	1.59	4.94	0.82	4.26	1.02	17.75	1.06	7.09	0.62	4.54	0.59
6163.9	0.57	0.21	2.62	0.76	0.96	1.55	5.85	0.75	3.92	1.07	2.02	0.88	1.56	0.58	0.57	0.55
6133.5	0.69	0.23	3.90	0.76	2.01	1.42	1.69	0.61	16.77	0.75	3.16	0.72	3.93	0.71	3.71	0.33
6109.2	3.86	0.27	3.59	0.63	7.13	1.73	11.18	0.75	3.35	0.62	16.31	0.72	3.33	0.69	5.61	0.34
6100.6	0.76	0.22	1.32	0.64	0.00	1.39	0.91	0.69	0.49	0.62	1.92	0.59	1.43	0.69	0.98	0.31
6092.1	0.54	0.26	0.33	0.87	0.00	1.43	0.19	0.87	−0.72	0.75	2.83	0.51	1.26	0.50	0.74	0.23
6082.8	6.95	0.30	0.24	0.81	3.85	1.64	6.45	0.92	5.61	0.73	10.21	0.57	6.18	0.56	4.83	0.23
6067.4	0.97	0.25	0.26	0.82	0.00	1.43	3.48	0.92	1.61	0.66	1.35	0.50	0.57	0.52	0.53	0.44
6056.3	0.91	0.40	2.86	0.53	2.14	1.59	1.92	0.85	2.14	0.94	−0.56	1.73	0.50	0.66	1.98	0.53
6046.0	8.16	0.46	6.05	0.76	1.12	1.42	10.03	0.94	5.07	0.78	15.92	0.64	1.95	0.65	2.41	0.75
6026.0	0.54	0.17	11.53	0.99	0.00	1.36	1.17	1.00	1.17	0.94	1.99	0.45	2.89	0.77	2.02	0.55
6017.0	0.26	0.17	0.87	0.94	0.00	1.36	0.70	1.17	0.22	1.05	0.97	0.75	1.15	0.77	1.10	0.52
6011.3	0.40	0.17	1.75	0.90	2.52	1.61	5.02	0.90	2.84	1.02	1.04	0.43	0.64	0.73	0.61	0.55
5989.8	1.83	0.23	0.90	0.48	2.47	1.62	1.82	0.57	5.33	1.01	5.78	0.82	5.84	0.73	2.51	0.42
5966.6	0.60	0.23	−0.12	0.48	0.00	1.38	4.65	0.57	3.59	1.02	0.85	0.74	0.01	0.64	0.90	0.35
5948.6	1.25	0.18	0.00	0.81	0.00	1.40	1.69	0.72	0.59	0.68	0.32	0.63	0.93	0.56	−0.27	0.35
5934.9	0.78	0.16	1.42	0.74	0.40	1.42	0.91	0.91	1.99	0.68	0.51	0.72	1.05	0.57	0.69	0.35
5927.1	1.31	0.19	2.39	0.68	0.16	1.23	3.64	0.69	1.10	0.72	3.83	0.67	6.72	0.61	1.81	0.35
5916.5	12.71	0.25	4.34	0.68	6.98	1.90	13.68	0.82	3.52	0.99	2.74	0.61	5.37	0.60	3.31	0.37
5906.5	1.08	0.20	4.12	0.70	1.46	1.59	3.22	0.81	1.06	1.01	1.24	0.63	1.22	0.56	2.18	0.40
5880.9	1.13	0.25	0.78	0.60	1.36	1.59	1.92	0.72	2.04	0.96	0.99	0.42	1.64	0.50	0.79	0.41
5847.7	0.50	0.21	1.16	0.61	1.24	1.43	2.73	0.72	0.52	0.92	3.58	0.43	2.00	0.52	2.24	0.41
5836.5	1.35	0.22	1.16	0.65	0.00	1.42	1.71	0.75	1.99	0.91	1.61	0.43	1.43	0.54	0.34	0.49
5820.4	0.67	0.23	0.53	0.65	1.52	1.61	3.48	0.85	−0.07	0.82	0.66	0.77	1.09	0.73	0.07	0.45
5812.2	2.94	0.24	1.76	0.64	1.51	1.62	3.72	0.81	1.20	0.59	0.15	0.51	4.26	0.78	0.74	0.44
5803.4	0.44	0.25	0.74	0.70	3.01	1.89	1.79	0.88	2.30	0.63	0.35	0.53	0.52	0.70	1.56	0.44

TABLE II *(Continued)*

E_γ (keV)	E_n=1.257 eV		E_n=46.7 eV		E_n=68.3 eV		E_n=95.6 eV		E_n=125.5 eV		E_n=154.2 eV		E_n=187.0 eV		530<E_n<907 eV	
	I	ΔI	I	ΔI	I	ΔI	I	ΔI	I	ΔI	I	ΔI	I	ΔI	I	ΔI
5797.8	4.54	0.26	1.15	0.80	0.30	1.43	1.95	0.79	4.10	0.89	0.77	0.54	2.29	0.69	3.41	0.44
5786.8	0.02	0.22	0.55	0.74	2.16	1.65	1.45	0.91	1.42	0.67	1.11	0.60	0.99	0.73	2.44	0.47
5766.6	0.55	0.18	0.97	0.57	0.00	1.45	1.87	0.75	3.17	0.87	3.12	0.54	0.79	0.57	2.10	0.55
5757.7	0.64	0.18	1.94	0.57	0.00	1.62	0.42	0.73	2.95	0.86	1.74	0.53	1.40	0.58	0.49	0.52
5743.0	0.79	0.20	0.08	0.36	2.13	1.70	−0.27	0.79	0.00	0.96	2.77	0.56	1.81	0.75	1.17	0.55
5734.0	0.18	0.18	3.57	1.29	1.02	1.67	0.51	0.60	4.46	0.29	1.82	0.45	1.05	0.61	1.13	0.57
5713.5	1.41	0.20	−0.23	0.91	1.18	1.33	0.85	0.85	1.61	0.86	1.99	0.57	1.64	0.71	0.74	0.61
5708.4	0.18	0.23	1.45	0.91	2.95	1.43	0.39	0.82	3.05	0.84	1.27	0.36	3.07	0.33	0.38	0.53
5695.1	1.13	0.18	0.55	0.73	0.00	1.46	5.17	0.91	2.20	0.83	8.53	0.86	4.06	0.40	1.65	0.50
5688.8	0.08	0.19	0.43	0.73	0.00	1.46	4.34	0.82	0.54	0.89	0.98	0.93	2.96	0.34	0.74	0.49
5674.1	2.47	0.21	0.13	0.81	2.89	1.73	2.06	0.78	1.48	0.54	0.57	0.78	2.58	0.34	1.01	0.52
5656.0	0.13	0.26	0.98	0.85	0.90	1.68	0.00	1.03	0.00	1.10	0.00	0.81	0.38	0.74	1.91	0.34
5648.3	0.25	0.17	2.75	0.99	1.80	1.71	2.10	1.09	2.30	0.52	3.77	0.82	2.45	0.56	0.30	0.35
5634.4	0.49	0.21	1.76	0.43	3.78	1.79	2.65	0.75	3.06	0.70	4.29	0.75	6.63	0.91	1.94	0.45
5616.5	3.79	0.26	4.54	0.43	2.32	1.76	2.56	0.72	2.47	0.57	2.21	0.63	1.07	0.79	0.89	0.45
5604.4	1.84	0.22	2.83	0.49	3.13	1.33	2.98	1.11	3.97	0.70	4.06	0.77	0.12	1.02	2.03	0.41
5587.9	1.18	0.23	6.95	0.97	0.00	1.40	2.39	0.88	3.03	0.49	1.07	0.60	1.60	0.56	1.58	0.41
5574.8	0.07	0.19	4.04	0.89	0.00	1.40	2.32	0.82	2.17	0.48	0.50	0.77	2.09	0.52	1.58	0.38
5566.1	−0.02	0.20	1.08	0.86	1.23	1.73	1.81	0.81	4.58	0.51	2.87	0.69	0.73	0.50	1.35	0.38
5546.6	2.03	0.21	0.07	0.87	1.74	1.56	0.31	0.88	0.00	1.15	2.63	0.43	8.22	0.61	0.66	0.40
5527.0	3.15	0.26	5.68	0.90	2.60	1.79	2.81	0.85	0.00	1.17	5.29	0.49	4.99	0.62	2.48	0.60
5521.0	4.79	0.26	1.15	0.82	2.94	1.80	2.51	0.82	2.22	0.72	2.52	0.45	0.00	0.79	1.38	0.70
5507.6	1.65	0.22	4.57	0.86	0.00	1.56	5.25	1.14	1.39	0.61	2.06	0.45	2.79	0.58	0.96	0.57
5493.6	0.67	0.23	0.72	0.76	0.00	1.55	1.29	0.81	1.39	0.61	2.00	0.49	0.42	0.61	1.38	0.64
5476.2	1.46	0.27	1.21	0.76	2.83	1.83	2.36	0.90	0.17	0.70	1.48	0.46	0.78	0.73	2.78	0.42
5472.5	0.18	0.30	−0.69	0.73	0.00	1.58	2.65	0.88	4.18	0.61	1.09	0.46	0.00	0.73	3.09	0.45
5463.3	2.50	0.31	2.27	0.72	3.73	1.70	0.61	0.79	1.02	0.61	0.71	0.49	1.18	0.73	3.89	0.40
5456.8	0.30	0.30	1.43	0.72	3.16	1.70	0.87	0.81	0.57	1.04	2.38	0.49	1.35	0.90	0.00	0.63
5453.3	0.00	0.27	0.00	0.94	0.00	1.59	−0.36	1.13	2.76	0.59	0.00	0.75	1.52	0.79	0.31	0.41
5441.4	0.00	0.30	2.73	0.80	2.41	1.83	−0.08	0.96	4.86	0.83	2.80	0.53	−0.26	0.53	0.37	0.53
5434.5	1.83	0.22	1.45	0.74	1.83	1.83	2.20	0.82	0.51	0.80	−0.20	0.50	1.19	0.52	1.51	0.52
5422.9	1.50	0.22	3.53	0.76	0.00	1.61	1.08	0.81	3.06	0.77	2.33	0.51	1.46	0.52	1.61	0.50
5413.5	1.39	0.23	1.49	0.76	3.00	1.87	4.02	0.91	1.85	0.77	0.32	0.51	2.17	0.56	0.97	0.53
5399.2	0.49	0.29	5.96	0.98	0.00	1.62	2.42	1.06	−0.16	1.27	2.13	0.72	0.82	0.33	1.64	0.45
5391.5	0.85	0.29	0.86	0.38	0.00	1.67	2.26	1.06	1.47	1.26	0.21	0.51	1.76	0.32	1.19	0.45
5364.5	0.90	0.29	0.49	0.74	0.00	1.68	3.69	0.99	2.26	1.02	1.02	1.00	2.08	0.61	1.44	0.52
5354.9	0.49	0.30	0.97	0.74	0.00	1.70	11.03	1.11	1.58	1.01	0.00	0.85	1.67	0.60	1.68	0.53
5346.5	14.72	0.36	6.50	0.81	6.39	2.04	8.85	1.09	5.87	1.26	9.58	1.46	5.04	0.61	5.28	0.53
5333.7	1.32	0.30	−0.33	0.77	5.00	2.02	3.54	1.02	1.99	1.02	1.50	0.77	3.37	0.65	0.25	0.81
5323.0	1.69	0.25	1.45	0.87	0.77	1.74	1.55	0.63	3.62	1.08	0.70	0.55	0.89	0.70	1.80	0.45
5311.5	0.89	0.23	2.01	0.82	0.00	1.73	0.00	1.17	4.43	0.97	1.53	0.54	0.70	0.66	1.79	0.42
5298.0	0.32	0.25	1.20	1.01	1.49	1.96	2.08	0.61	1.52	0.97	2.28	0.56	0.14	0.66	1.61	0.42
5266.4	9.12	0.29	3.24	0.57	3.47	2.05	8.24	1.24	4.61	0.54	2.39	0.78	0.61	0.67	3.36	0.35
5257.3	1.14	0.26	3.34	0.59	0.00	1.76	2.98	1.17	7.72	0.57	1.61	0.79	1.18	0.60	0.82	0.34
5251.0	1.24	0.25	1.37	0.63	2.10	2.02	0.76	1.17	3.71	0.57	−0.21	0.85	0.79	0.62	1.34	0.35
5237.7	1.95	0.29	4.56	0.77	2.35	2.04	2.35	1.15	2.39	0.80	4.93	0.82	0.50	0.65	2.24	0.59
5223.1	0.76	0.32	−0.56	0.73	0.00	1.80	1.32	1.43	0.62	0.75	0.35	0.70	2.33	0.69	0.91	0.55
5217.6	1.16	0.35	1.28	0.73	0.00	1.80	3.75	1.36	2.18	0.75	0.00	0.90	1.50	0.66	1.34	0.55
5203.8	5.25	0.27	2.14	0.74	2.26	2.05	6.32	1.21	4.00	0.80	2.37	0.72	0.74	0.65	1.71	0.56
5186.8	0.99	0.24	1.74	1.11	0.00	1.80	2.26	0.93	−0.83	1.13	2.23	0.57	1.20	0.66	0.72	0.41
5180.2	0.56	0.26	1.58	1.10	0.00	1.82	2.47	0.93	0.94	1.15	2.95	0.57	0.90	0.69	0.35	0.93
5173.1	1.27	0.26	1.02	1.33	3.01	2.11	4.19	0.93	0.87	1.18	−1.10	0.85	3.31	0.86	1.73	0.74
5152.8	5.66	0.29	3.20	0.74	10.86	2.15	1.82	1.17	3.68	1.07	0.59	0.43	0.07	0.61	2.55	0.44
5142.9	0.81	0.29	−0.68	0.80	2.18	1.86	3.02	1.38	0.94	1.52	0.00	0.93	1.59	0.60	0.19	0.41
5133.6	1.02	0.29	0.52	0.77	3.29	2.04	1.61	1.29	3.52	1.24	3.17	0.46	2.10	0.62	1.25	0.42
5123.4	0.31	0.26	2.41	0.76	2.91	2.13	2.02	1.21	0.78	1.16	2.65	0.50	0.12	0.65	0.34	0.44
5106.9	2.06	0.33	3.07	0.72	0.00	1.86	1.15	0.85	1.82	0.63	5.67	0.67	0.66	0.77	1.42	0.52
5094.0	0.97	0.31	2.60	0.80	3.82	2.18	4.38	0.88	1.87	1.37	10.80	0.68	2.41	0.75	0.94	0.50

TABLE II *(Continued)*

E_γ (keV)	E_n=1.257 eV		E_n=46.7 eV		E_n=68.3 eV		E_n=95.6 eV		E_n=125.5 eV		E_n=154.2 eV		E_n=187.0 eV		530<E_n<907 eV	
	I	ΔI	I	ΔI	I	ΔI	I	ΔI	I	ΔI	I	ΔI	I	ΔI	I	ΔI
5082.2	0.52	0.32	2.41	0.80	0.00	1.87	4.55	0.91	1.82	0.64	5.79	0.67	0.64	0.75	2.13	0.55
5070.0	1.54	0.35	3.80	0.82	2.33	2.16	1.33	0.96	2.25	1.42	3.02	0.75	0.08	0.91	1.80	0.57
5060.2	0.70	0.23	3.04	0.43	0.92	1.95	1.04	1.20	3.99	1.74	2.05	0.63	3.31	0.82	0.40	0.53
5036.9	0.36	0.29	2.47	0.97	0.00	1.96	−0.58	1.35	1.77	0.80	−0.71	1.20	−0.90	0.97	1.38	0.57
5031.4	0.55	0.29	−1.37	0.93	0.00	1.92	4.13	1.33	0.19	0.75	1.28	1.17	0.91	0.98	1.50	0.96
5020.9	3.71	0.26	0.52	0.87	0.00	1.93	4.26	1.17	2.57	0.68	1.14	0.63	0.79	1.50	1.58	0.86
5004.3	2.24	0.32	3.24	0.98	1.58	1.98	1.87	1.38	2.49	0.75	4.69	0.68	−0.73	0.93	1.42	0.56
4978.3	0.00	0.30	0.00	1.20	1.27	1.98	2.83	0.81	2.93	0.64	1.66	0.82	1.99	0.65	1.20	0.56
4972.7	2.00	0.23	2.27	1.12	3.11	2.07	3.01	0.94	4.13	0.67	4.75	0.82	0.54	0.73	0.14	1.02
4960.8	0.89	0.25	0.90	0.72	0.00	1.99	2.26	0.96	3.54	0.67	0.33	0.79	0.17	0.69	1.98	0.79
4950.0	0.75	0.23	0.68	0.48	0.00	1.99	3.25	1.27	0.00	1.45	6.44	0.87	3.80	0.67	0.83	0.81
4923.0	2.33	0.39	0.78	0.64	1.73	2.05	2.89	0.94	6.43	1.15	2.88	0.98	1.20	0.62	2.80	0.63
4913.6	4.25	0.38	2.84	1.29	6.76	2.39	4.89	0.93	10.43	1.17	2.67	0.93	4.06	0.65	3.11	0.60
4900.6	2.30	0.36	3.51	0.97	0.00	2.04	5.20	0.96	1.55	1.10	0.36	0.93	1.32	0.61	2.85	0.60
4890.8	0.44	0.37	0.65	1.24	0.49	2.30	0.60	1.20	0.49	1.17	2.39	1.02	1.97	0.66	2.17	1.08
4863.2	1.41	0.33	1.47	1.17	1.61	2.07	1.56	1.75	0.99	0.67	3.87	0.68	0.87	0.71	0.64	0.63
4858.2	1.53	0.32	0.73	1.17	2.68	2.21	2.26	1.87	1.45	1.52	2.42	0.71	0.97	0.67	1.83	0.56
4848.2	1.34	0.35	3.14	1.10	0.00	2.10	−0.10	1.11	−0.32	0.73	1.37	0.61	1.19	0.66	1.85	0.55
4838.7	0.43	0.50	−1.03	1.24	2.64	2.41	1.24	1.18	4.56	0.82	1.20	0.63	0.74	1.01	2.21	0.53
4834.1	3.52	0.53	3.82	1.32	0.00	2.11	0.21	1.17	2.25	0.96	−1.31	0.53	2.75	0.70	1.38	0.53
4824.3	0.42	0.46	2.05	1.10	0.00	2.13	4.05	1.15	3.11	0.78	0.50	0.56	0.79	0.74	0.55	0.59
4811.8	0.94	0.31	1.68	0.98	0.00	2.14	2.38	1.11	0.30	0.87	2.31	1.19	2.59	0.53	0.20	0.68
4800.6	0.64	0.24	0.12	0.98	0.00	2.18	1.30	0.90	3.41	0.91	1.46	1.28	1.57	0.67	1.65	0.60
4778.6	2.25	0.45	0.74	0.69	0.00	2.25	−0.21	1.11	3.27	0.82	7.46	0.95	6.10	0.85	1.57	0.59
4773.4	0.63	0.57	1.53	0.69	0.00	2.27	1.77	1.12	2.95	0.82	0.00	0.81	0.00	1.15	1.35	0.75
4765.5	0.57	0.37	2.84	0.70	3.63	2.51	0.73	1.15	3.01	0.83	3.86	0.96	1.28	1.05	1.31	0.75
4751.1	0.73	0.30	4.97	1.10	4.75	2.52	0.75	0.90	2.89	1.05	0.14	0.78	−0.74	0.86	2.05	0.64
4743.3	1.13	0.30	3.21	1.09	0.00	2.20	2.51	0.88	0.70	0.97	0.14	0.77	3.77	1.19	1.10	0.63
4735.2	0.70	0.32	1.64	0.98	0.00	2.21	1.39	0.82	2.14	0.97	−0.50	0.74	3.15	1.19	1.90	0.56
4724.9	3.32	0.31	1.92	1.10	0.00	2.21	3.23	0.91	1.18	1.05	2.10	0.79	3.64	0.61	1.69	0.56

in each case, populated by high-energy γ emission.

Greenwood[15] suggested a 3^- or 3^+ state at 269 keV. A state at 268.0 keV is populated weakly from the 1^- levels but not from the 0^- levels. This could indicate that this is a 3^- state involving an $E2$ transition, the probability of emission for an $M2$ transition to 3^+ being negligible.

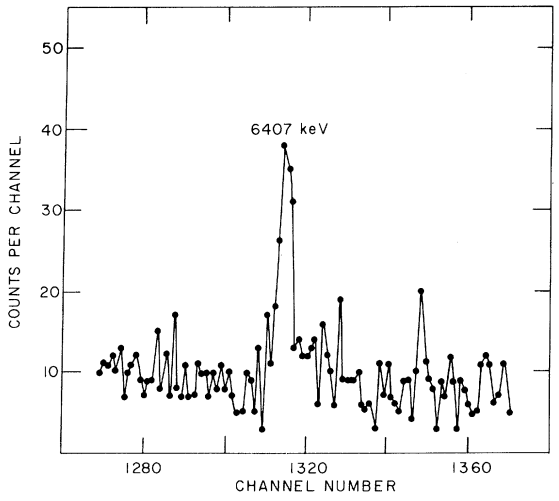

FIG. 6. γ-ray spectra for the p-wave resonance-neutron capture in rhodium (E_n = 34.4 eV).

As mentioned earlier, the strongest transition from the p-wave 34.4-eV resonance is the 6407-keV line. This populates a final state at 592 keV which would be a negative-parity state, assuming an $E1$ character for this transition. The transition is also seen weakly in the spectrum of the 0^- 154.3-eV resonance. This limits the spin of the final state to either 1^- or 2^-.

VI. DISCUSSION OF RESULTS

A. Low-Lying States in Rh^{104}

The density of levels is seen to be high at low excitation energies. This high density is expected for this nucleus, since the proton and neutron configurations lead to a large number of possible states at fairly low energies. The ground-state shell-model configuration of Rh^{104} with 45 protons and 59 neutrons has been suggested by Greenwood[15] as $(\pi g_{9/2})^5{}_{7/2}\nu d_{5/2}$. Groshev *et al.*[4] suggest either this configuration as proposed by Greenwood or the alternative configuration $(\pi g_{9/2})^5{}_{9/2}\nu g_{7/2}$. Six states of spin 1^+ to 6^+ belong to the first configuration,

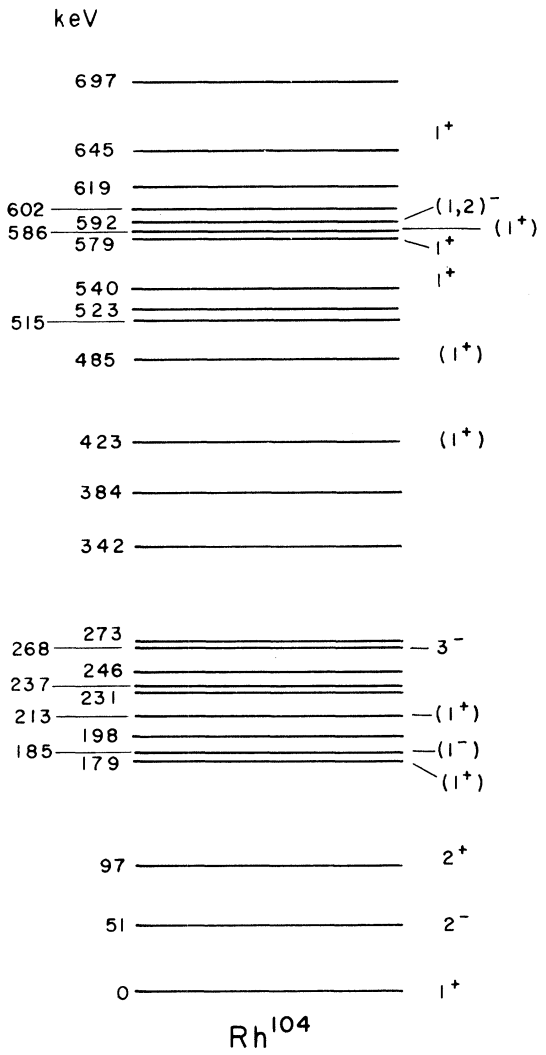

FIG. 7. Low-lying energy levels of Rh^{104} as determined from the present measurements.

while eight states with spins 1^+ to 8^+ would belong to the second suggested configuration. Moreover, many of the large number of states belonging to the configuration $(\pi g_{9/2})^5{}_j \nu d_{5/2}$ or $(\pi g_{9/2})^5{}_j \nu g_{7/2}$, where j takes on one of 12 values ranging from $\frac{1}{2}$ to $\frac{25}{2}$ formed through 20 possible combinations, will have relatively low energies.

Low-lying negative-parity states arise from the configuration $(\pi p_{1/2})^{-1}(\pi g_{9/2})^6{}_0 \nu d_{5/2}$ which would lead to two states of spin 2^- and 3^-, or the alternative configuration $(\pi p_{1/2})^{-1}(\pi g_{9/2})^6{}_0 \nu g_{7/2}$ which leads to 3^- and 4^- states. The lowest observed negative-parity state is the 2^- first excited state at 51 keV. This seems to indicate that the first configuration is the one applicable in this case. The 3^- state at 268 keV could be the second member of this configuration. Higher-energy negative-parity states may arise from the neutron configuration $\nu h_{11/2}$.

B. Determination of Statistical Parameters

The number of degrees of freedom (ν) of the distribution of partial radiative widths can be obtained by plotting the cumulative probability distribution of the reduced partial radiation widths ($\Gamma_{\lambda\gamma f} E_\gamma{}^{-3}$) and comparing the plot with the theoretical curves for the χ^2 distributions with different degrees of freedom. However, in order to take into account the effect of the limited sample size and experimental errors, a ν value is obtained using a maximum-likelihood method, which includes such effects.[16] If x_{ij}, the partial widths normalized to unit mean for the final state i over resonance j, are assumed to belong to a χ^2 distribution with $\nu = 2\rho$ degrees of freedom, then the likelihood function $L(x_{ij}, \rho)$ is defined as

$$L(x_{ij}, \rho) = \prod_{ij} \frac{\rho^\rho}{\Gamma(\rho)} x_{ij}{}^{\rho-1} e^{-\rho x_{ij}} .$$

The number of degrees of freedom is then determined by solving for the ρ which maximizes the above expression.

Since measured widths include zero or negative values for which the logarithm of the likelihood function diverges and is undefined, the sample is truncated at a value determined by the median of its normalized error distribution. Values smaller than the cutoff value are set equal to one half of the cutoff value.

In order to test the hypothesis that the physical sample is drawn from the χ^2 distribution with ν_0 degrees of freedom, a Monte Carlo method is used. A mathematical sample of the same size as the physical sample is drawn randomly from a χ^2 distribution with ν_0 degrees of freedom. Errors drawn from a normal distribution with unit standard deviation and zero mean are then added to the mathematical sample. This sample is then treated as the physical sample, and the mathematical number of degrees of freedom ν_m is determined. The process is repeated 100 times and the distribution of ν_m is plotted. If ν_p lies within the 10 and 90% limits of this distribution, then the data are said to be consistent with ν_0 degrees of freedom. In order to determine the best value of ν the process is repeated for different values of ν_0, and the probability that ν_m is larger than ν_p is plotted as a function of ν_0. The best value for ν is taken as the one corresponding to 0.50 on this plot. The lower and upper limits are the values corresponding to 0.10 and 0.90 on the plot. The distribution of the partial radiation widths was studied assuming a χ^2 distribution, using the maximum-likelihood method described above.

The application of this method is not hampered by lack of knowledge of most of the final-state

spins and parities. The distribution of partial widths over the resonances can be examined by combining all 145 final states reported here after normalizing the transitions to unit mean for each final state. On this basis, γ rays of either $E1$ or $M1$ character can contribute to the distribution. The results of the maximum-likelihood analysis are shown in Fig. 8:

spin-0 resonances $\nu = 2.70^{+0.53}_{-0.40}$,

spin-1 resonances $\nu = 2.45^{+0.38}_{-0.40}$.

Three spin-0 and four spin-1 resonances are included in the above results. The 68.3-eV resonance was arbitrarily assigned spin 1; the deletion of this resonance has no appreciable effect on the observed value for ν.

These data are clearly inconsistent with the Porter-Thomas distribution. Such deviations from the Porter-Thomas distribution have been observed in a number of other nuclei.[17]

In order to explain such deviations from the Porter-Thomas distribution, Beer[18] extended a model originally proposed by Rosenzweig[19] in a manner which would allow ν values greater than 1 for the distribution of partial radiation widths while allowing a ν value of 1 for the distribution of reduced neutron widths. This model assumes that the compound-nucleus levels can be expanded in terms of two groups of orthogonal sets of states, one having a large number and the other a smaller number of members, with the further assumption that only the large set contributes to the reduced neutron widths, while both groups contribute to the partial radiation widths. The physical interpretation of this mathematical construction is not completely clear. It is attractive, however, to associate the large set with the class of single-particle states, while the smaller set can be associated with the set of doorway or 2p-1h states.

C. Spectral Shape

Figure 3 shows, as has been noted previously by Groshev *et al.*,[4] that the transitions to states of about 1-MeV excitation are enhanced in thermal capture relative to the rest of the spectrum. The thermal capture is dominated by a single resonance (the 1.257 eV) and since it is known that resonance spectra show large fluctuations in intensity, it is necessary to investigate such effects after averaging over a large number of resonances. The γ-ray spectrum of the neutron time-of-flight peak corresponding to neutron energy range 530 to 900 eV was considered to satisfy this condition, since a large number of resonances contribute to the capture in this region. The spectrum of this group of resonances still shows the enhancement of transitions mentioned above. Actually, all spectra of individual resonances show the same effect and although the enhanced transitions vary from one resonance to another, these enhanced lines fall in the same γ-ray energy region.

Figure 9 shows the distribution of the reduced widths, summed over intervals of 200 keV, as a function of energy (the solid line). Owing to the high density of levels, the number of observed transitions cannot be used to study the variation of the average reduced width with energy. However, the level density for medium and heavy nuclei can be expressed as $e^{E_x/T}$, where E_x is the excitation energy and T is the nuclear temperature. This expression with $T = 1$ MeV was used in determining the average reduced widths plotted in Fig. 9 (the dashed line). This last plot shows that the average

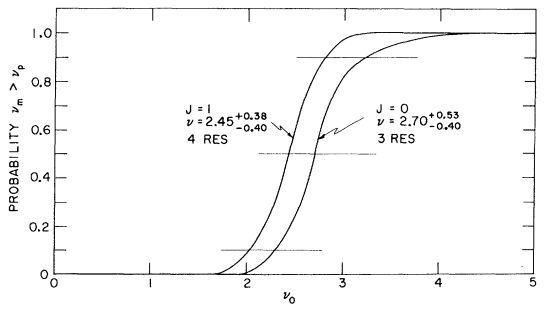

FIG. 8. ν value for the statistical distribution of observed partial radiation widths from neutron-resonance capture in rhodium. Transitions from spin 0 and 1. Resonances are analyzed separately.

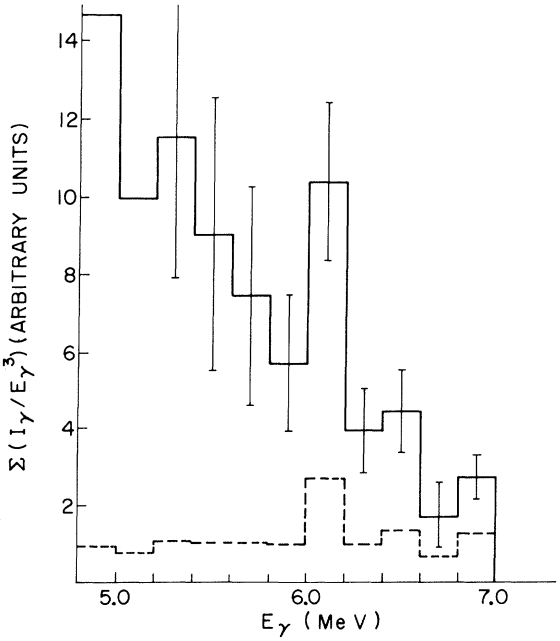

FIG. 9. Distribution of reduced transition probabilities of γ rays emitted in the resonance-neutron capture in rhodium.

partial radiation width follows an E_γ^3 energy dependence except for the γ rays in the range 6–6.2 MeV corresponding to final states of excitation energy 0.8–1.0 MeV. Groshev *et al.*[4] suggested that this enhancement is due to direct capture, assuming that the final states are p-wave neutron states. HKP[6] offer the alternative explanation of the existence of a giant $M1$ resonance which is responsible for this enhancement, as suggested by Bergqvist, Lundberg, and Starfelt.[20]

Since the capture studied here is resonance capture, with thermal capture included since it is dominated by the 1.257-eV resonance, we should expect the resonance channel capture to be the dominant mode of the single-particle contribution to the reaction, rather than the direct-capture process. Channel capture leads to a correlation between (d,p) and (n,γ) intensities and a correlation between partial radiation widths and reduced neutron widths. There is no detailed study of the (d,p) reaction for Rh. However, the correlation coefficient for the partial radiation widths and the reduced neutron widths was calculated and averaged over 17 final states within the range of 0.8–1.0-MeV excitation energy. This average correlation coefficient was found to be 0.17 for 0^- resonances and 0.003 for 1^- resonances. Both of these values are consistent with zero correlation. This indicates that channel capture cannot be a dominant mode of the reaction leading to final states in this region.

Earle, Lone, and Bartholomew[21] have suggested that similar enhancement regions in the spectra of other nuclei could arise from p-h annihilation processes following the formation of doorway states. The ground-state proton configuration for the target nucleus Rh^{103} is $(\pi p_{1/2})^{-1}(\pi g_{9/2})^6{}_0$. The low-lying neutron states that are available are all positive-parity states. These are the $d_{5/2}$, $s_{1/2}$, $g_{7/2}$, and $d_{3/2}$ states (not necessarily in this order). It is possible to form a 2p-1h state which subsequently decays to a single-particle state through the annihilation of a p-h pair with the emission of a γ ray of dipole multipolarity only by assuming that a $g_{9/2}$ proton is excited to the $g_{7/2}$ orbit as a result of its collision with the $s_{1/2}$ incoming neutron and that the neutron occupies a $d_{3/2}$ or $s_{1/2}$ orbit. This 2p-1h state can decay to a single-particle state by the transition of the proton from the $g_{7/2}$ to the $g_{9/2}$ orbit, which is a spin-flip process. This will lead to an $M1$ multipolarity for the emitted photon. It is not possible to construct 2p-1h states which conserve both the energy and parity of the system and which can decay by the emission of $E1$ radiation. Thus, if this effect is the one responsible for the enhancement of the transition strength, then we expect the states in the range 0.8 to 1.0 MeV to be populated in the (d,p) reaction since they preserve the Rh^{103} core, and furthermore, we expect that the orbital angular momentum of the transferred neutron must be even, since the reasoning we have followed implies that the enhanced γ-ray transitions consist primarily of $M1$ radiation.

The only (d,p) study in Rh that is available at present is that of Da Silva and Buechner,[22] which only lists the energies of the states that are populated in the reaction. Of the 17 states that are observed in the (n,γ) reaction in the region of the "bump" near 1 MeV, nine states are seen to be populated in (d,p). Transitions to these nine states show a correlation between the partial radiation widths and the reduced neutron widths. The correlation coefficient averaged over the nine final states is found to be 0.47, which falls at the 0.99 point of the normal distribution. This correlation does not necessarily indicate the dominance of single-particle effects, since from the shell-model structure of the low-lying states in Rh^{104}, one would expect the neutron p states to be close to the neutron binding energy rather than near 1-MeV excitation.

Such large correlations between partial radiation widths and reduced neutron widths are also observed for final states which cannot be reached by a single-particle process. For example, the partial radiation widths for the strong transitions populating the 1^+ state at 213 keV are seen to be highly correlated with the reduced neutron widths. A correlation coefficient of 0.99 was obtained in this case. Since this state is a positive-parity state, it is assumed to have the proton configuration $(\pi g_{9/2})^5{}_j$, which involves the transfer of one proton from the $\pi g_{9/2}$ orbit to the $\pi p_{1/2}$ orbit, which has only one proton in the ground state of the target nucleus Rh^{103}. Thus, the population of this state does not preserve the Rh^{103} core. This is borne out by the fact that this state is not populated in the (d,p) reaction. The significance of the large correlation coefficient between the partial radiative widths and the reduced neutron widths for this case is not clear.

The strength of the transitions populating this final state could be explained in terms of the dominance of the decay of doorway states to more simple configurations through the emission of $E1$ radiation. This process will involve a transition between the configurations

$$(\pi p_{1/2})^{-1}(\pi g_{9/2})^5{}_{9/2}\pi d_{3/2}\nu g_{7/2} \quad (\pi g_{9/2})^5{}_{9/2}\nu g_{7/2}\,,$$

or

$$(\pi p_{1/2})^{-1}(\pi g_{9/2})^5{}_{7/2}\pi d_{3/2}\nu d_{5/2} \quad (\pi g_{9/2})^5{}_{7/2}\nu d_{5/2}\,,$$

thus, assuming that an $E1$ photon is emitted due to the annihilation of the $d_{3/2}$ proton and the proton

$p_{1/2}$ hole.

To summarize, it has been shown that the enhancement of transitions in the "bump" region cannot be due to single-particle effects and that this enhancement can be due to doorway state effects only if the transitions are of $M1$ multipolarity.

The multipolarity could be determined from the study of the $Rh^{103}(d,p)Rh^{104}$ reaction, which would determine the parity of the final states. If these states prove to be of positive parity, thus leading to $E1$ multipolarity for the radiative transitions, we would expect that processes more complex than the single-particle or two-step doorway-state effects are the dominant modes of the capture process.

---

†Work supported by the U. S. Atomic Energy Commission.

*Submitted in partial fulfillment of the Ph.D. thesis, State University of New York at Albany. Present address: University of Jordan, Amman, Jordan.

[1]U. Gruber, Z. Physik 178, 472 (1964).

[2]A. S. Melioranskii, L. F. Kalinkin, and I. V. Estulin, Izv. Akad. Nauk SSSR Ser. Fiz. 28, 1010 (1964) [transl.: Bull. Acad. Sci. USSR, Phys. Ser. 28, 1012 (1964)].

[3]O. Schult, private communication.

[4]L. V. Groshev, A. M. Demidov, G. A. Kotel'nikov, V. N. Lutsenko, and V. I. Pelekhov, Izv. Akad. Nauk SSSR Ser. Fiz. 28, 1118 (1964) [transl.: Bull. Acad. Sci. USSR, Phys. Ser. 28, 1021 (1964)].

[5]N. C. Rasmussen, Y. Hukai, T. Inouye, and V. J. Orphan, Air Force Cambridge Research Laboratory Report No. AFCRL-69-0071, 1969 (unpublished).

[6]L. B. Hughes, T. J. Kennett, and W. V. Prestwich, Can. J. Phys. 44, 2041 (1966).

[7]R. E. Chrien and M. Reich, Nucl. Instr. Methods 53, 93 (1967).

[8]*Neutron Cross Sections,* compiled by M. D. Goldberg, S. F. Mughabghab, S. N. Purohit, B. A. Magurno, and V. M. May, Brookhaven National Laboratory Report No. BNL 325 (U. S. Government Printing Office, Washington, D. C., 1966), 2nd ed., Suppl. No. 2.

[9]M. A. Lone, R. E. Chrien, O. A. Wasson, M. Beer, M. R. Bhat, and H. R. Muether, Phys. Rev. 174, 1512 (1968).

[10]W. Kane and M. Mariscotti, private communication.

[11]R. C. Greenwood, Phys. Rev. 129, 339 (1963).

[12]J. Trochon, A. Lottin, and P. Rubin, Compt. Rend. B262, 507 (1966).

[13]Nai-yen Wang *et al.*, Zh. Eksperim. i Teor. Fiz. 45, 1743 (1963) [transl.: Soviet Phys.–JETP 18, 1194 (1964)].

[14]G. A. Bartholomew *et al.*, Nucl. Data A3, 367 (1967).

[15]R. C. Greenwood, Phys. Rev. 129, 345 (1963).

[16]D. L. Price *et al.*, Nucl. Phys. A121, 630 (1968).

[17]R. E. Chrien, *Neutron Capture Gamma-Ray Spectroscopy* (International Atomic Energy Agency, Vienna, Austria, 1969), p. 627.

[18]M. Beer, Ph.D. thesis, State University of New York, Stony Brook, 1968 (unpublished).

[19]N. Rosenzweig, Phys. Rev. Letters 6, 123 (1963).

[20]I. Bergqvist, B. Lundberg, and N. Starfelt, Argonne National Laboratory Report No. ANL 6797, 1963 (unpublished).

[21]E. D. Earle, M. A. Lone, and G. A. Bartholomew, Bull. Am. Phys. Soc. 14, 515 (1969).

[22]A. G. DaSilva and W. W. Buechner, Bull. Am. Phys. Soc. 7, 83 (1962).